02

Effect of Yttrium Content on Luminescent Properties of $HfO_2-Y_2O_3-Eu_2O_3$ Cubic Ceramics

© E.V. Dementeva, G.A. Gusev, P.A. Dementev, M.A. Yagovkina, M.V. Zamoryanskaya

Ioffe Institute,
St. Petersburg, Russia

e-mail: dementeva@mail.ioffe.ru

Received: December 02, 2024
Revised December 02, 2024
Accepted December 10, 2024

The luminescent properties of $HfO_2-Y_2O_3$-Eu_2O_3 ceramics with different yttrium content, prepared by coprecipitation from a common solution with subsequent sintering and additional annealing in an argon atmosphere, were studied. It was shown that the ceramics have a cubic crystal structure, the average grain size is about $2-4\,\mu$m. An increase in the yttrium content leads to an increase in the lattice constant, as well as to an increase in the number of low-symmetry Eu^{3+} positions.

Keywords: YSH, Eu^{3+}, ceramics, cathodoluminescence.

DOI: 10.61011/EOS.2025.01.60562.7408-24

Introduction

The ceramic materials are of great practical interest and applied in various fields of science and technics. Recently, much attention has been paid to the research of ceramics based on cubic zirconium and hafnium oxides stabilized with trivalent ions, for example, yttrium Y and/or lanthanides. A number of studies have been devoted to investigation of luminescent properties of the Y-stabilized ceramics based on ZrO_2 (YSZ), which is co-doped by the ion oxides of trivalent metals [1–4]. Since zirconium oxide, stabilized in the cubic phase, has a unique chemical, thermal and radiation resistance, this ceramics continues to be the focus of research for use as thermal barrier coatings [5–7]. Also among possible applications of Y-stabilized ZrO_2 ceramics is the development of ionizing radiation sensors which operate based on the thermal luminescence effect. The thermal luminescent properties of YSZ ceramics activated by the rare-earth ions of Eu [8] and Er [9] are of specific interest to the researchers.

Hafnium is a chemical analog of zirconium, but hafnium oxide, stabilized in the cubic phase, is much less studied. Europium will be used to activate ceramics, since Eu^{3+} has a bright luminescence in the red region of the spectrum, and its spectra are sensitive to the local symmetry [10].

The purpose of this study — to synthesize HfO_2-Y_2O_3-Eu_2O_3 ceramics with various yttrium content and define its effect on the crystalline structure and luminescent properties.

Sample synthesis and study methods

4 precursor of HfO_2-Y_2O_3-Eu_2O_3 with various yttrium content were obtained by method of co-precipitation. The ceramics were synthesized for 3 h at a temperature of 1500°C. The samples were sawn, fixed in epoxy resin, and a carbon film was sprayed onto their surface to ensure electron flow drain for the electron probe microanalyzer (EPMA) and cathodoluminescence (CL) studies. Further individual samples will be shortly designated as xY, where x — planned contents of yttrium (form. units).

The elemental composition of the studied samples was obtained by EPMA. The study of the composition was carried out on a CAMEBAX electron probe microanalyzer equipped with four X-ray spectrometers with the following electron beam parameters: electrons energy $U = 20$ keV, absorbed current $I = 15$ nA, beam diameter $d = 2\,\mu$m. For analysis, the analytical line $L\alpha$ was chosen for all elements. The standards selected included metallic hafnium (for Hf), $Y_3Al_5O_{12}$ compounds (for determination of Y) and $EuPO_4$ (for defining Eu). The oxygen content was calculated based on stoichiometry. The elemental composition was measured in several (minimum five) randomly selected areas of the samples.

All samples were examined by X-ray diffraction phase analysis (XRD). NaCl powder was used as an internal standard for determining structural parameters. The measurements were performed on diffractometer D2 (Bruker, Germany) ($\lambda = 1.5406$ Å, 30 kV, 10 mA), equipped with PSD camera and LENXEYE detector.

The surface relief was studied using NTegra-Aura atomic-force microscopy (NTMDT-SI, Moscow, Russia) by means of standard silicon probes (rigidity ~ 4 N/m, typical radius of the probe tip rounding ~ 10 nm). The measurement were done in a semi-contact mode in air.

The luminescent properties of the ceramics samples were studied by cathodoluminescence (CL) method using the same CAMEBAX setup, additionally equipped with an optical spectrometer. The spectra of CL samples were obtained

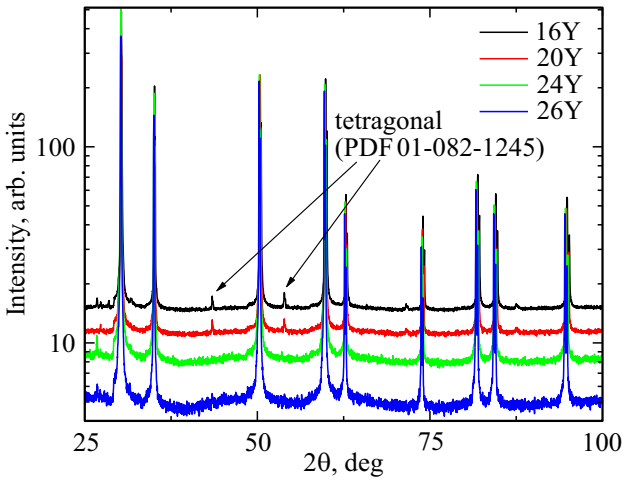

Figure 1. XRD patterns obtained for ceramics HfO_2-Y_2O_3-Eu_2O_3.

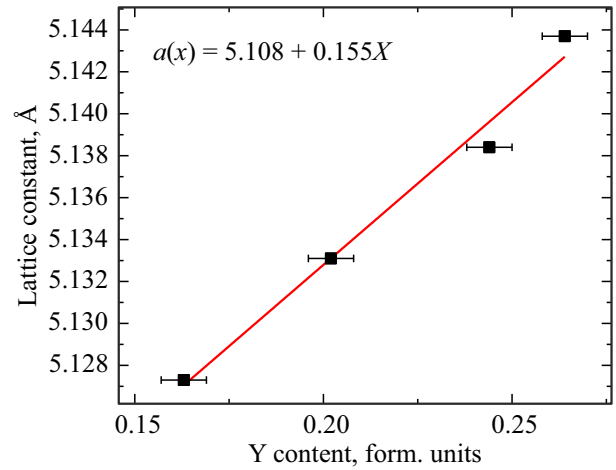

Figure 2. Lattice constant versus yttrium content in the cubic phase of ceramics HfO_2-Y_2O_3–Eu_2O_3.

within the wavelength range of $\lambda = 350–800$ nm: electron beam energy $U = 20$ keV, absorbed current $I = 20$ nA and the beam diameter $d = 5\,\mu$m. The CL images of the samples were obtained under the following conditions: electron beam energy $U = 20$ keV, absorbed current $I = 100$ nA and beam diameter $d = 200\,\mu$m. The decay times were obtained for the most intense transition $^5D_0–^7F_1$. Time measurements were carried out at the diameter of the electron beam 40 μm, since measurements with a smaller diameter led to a greater spread of the determined parameters [11].

Study results

The average ultimate composition of samples was obtained by EPMA method (Table 1). The obtained values of the elements content corresponded to the planned ones, the deviation did not exceed the measurement error limits for all samples (10% for europium, 2% for other elements in the samples). The homogeneity of the composition

Table 1. Elemental composition of samples according to EPMA data

Name sample	Element content in form. units		
	Hf	Y	Eu
16Y	0.82±0.01	0.163±0.006	0.016±0.001
20Y	0.786±0.005	0.200±0.006	0.014±0.001
24Y	0.74±0.01	0.244±0.006	0.016±0.001
26Y	0.72±0.02	0.264±0.006	0.016±0.001

was investigated for all samples of the series, and it was shown that yttrium is distributed uniformly in the selected concentration range.

Fig. 1 illustrates the XRD patterns obtained for all samples. It is demonstrated that cubic phase (PDF 01-077-2286) was prevailing for all samples. In samples 16Y and 20Y an impurity of tetragonal phase is observed (PDF 01-082-1245).

The lattice constant for the cubic phase was determined for all samples and its dependence on the yttrium content was constructed (Fig. 2). The lattice constant increases almost linearly with higher yttrium content: $a(x) = 5.108 + 0.155x$. The deviation from the linear dependence may be due to the heterogeneity of the yttrium distribution in the sample, the value of which lies within the measurement error of EPMA method. A monotonous increase in the lattice constant indicates the successful formation of a solid solution.

The AFM topography study showed that the ceramic surface mainly consists of sintered grains with a resulting characteristic size of about 10 μm (Fig. 3, *a*). The presence of grooves on the surface makes it possible to estimate the initial grain size — 2–4 μm. A more detailed study of the surface showed that ceramic grains are based on particles with a characteristic size 50–100 nm (Fig. 3, *b*).

The obtained CL-images are presented in Fig. 4. It can be seen that all samples have a uniform red luminescence, and the nonuniformity of luminescence is related only to the surface relief, except for sample 16Y, in which areas with white luminescence ranging in size from 40 to 200 μm are observed. The CL spectra of all samples contain emission bands associated with transitions in Eu^{3+} ions, including high-energy transitions ($^5D_0–^7F_j$, $^5D_1–^7F_j$, and $^5D_2–^7F_j$). The intensity ratios of the bands and their positions are characteristic of hafnium oxide with a cubic crystal structure [12,13]. In CL spectrum of 16Y sample there's an additional band with an emission maximum of 615 nm. This band is associated with the splitting of $^5D_0–^7F_2$ transition levels, which occurs in lower-symmetric phases of hafnium oxide, for example, in the tetragonal phase [13].

The nature of the contrast in CL image for sample 16Y was investigated in detail (Fig. 5). In CL spectrum

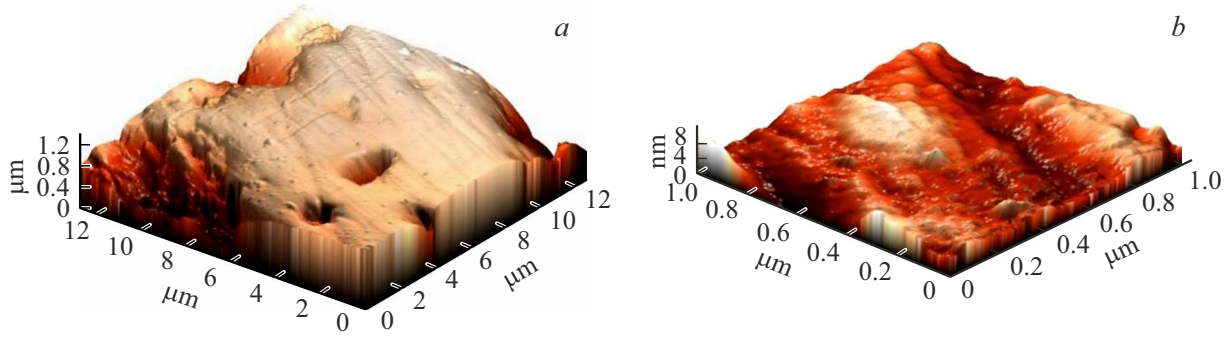

Figure 3. AFM images on the ceramics surface 20Y: (*a*) scanning field 13 × 13 μm, (*b*) scanning field 1 × 1 μm.

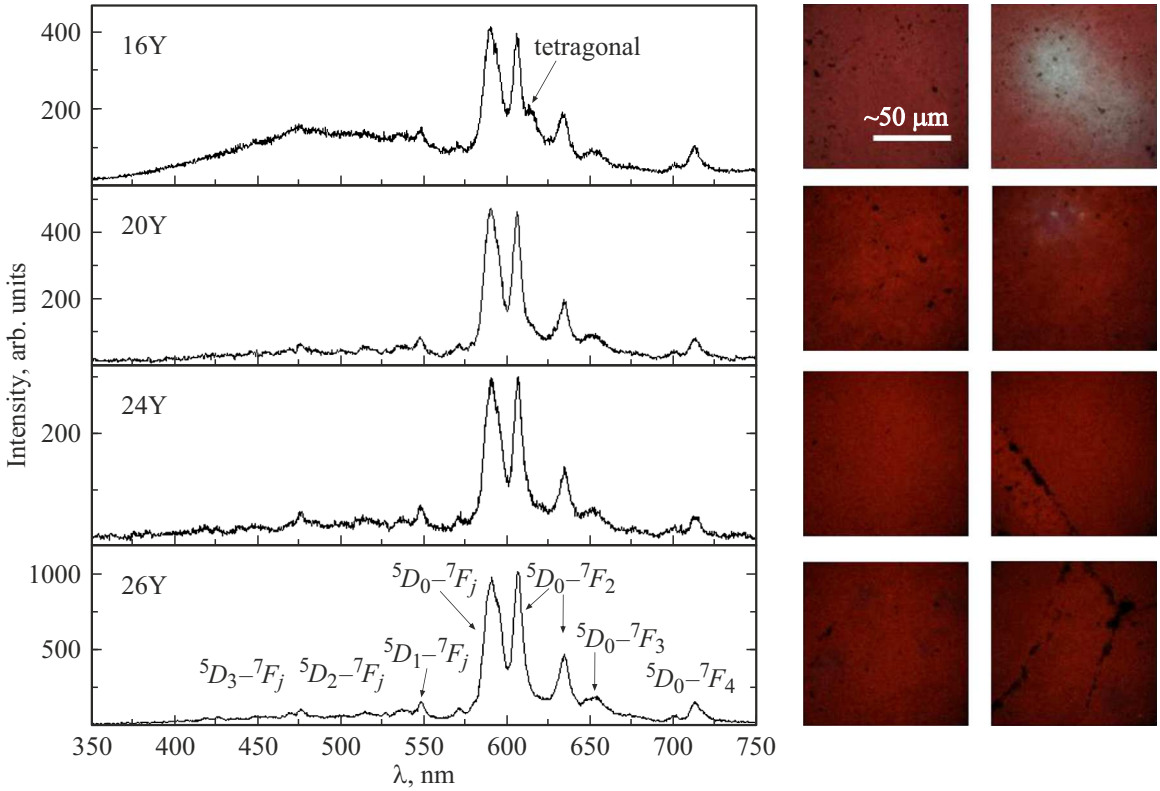

Figure 4. Spectra and CL images of ceramics with various content of yttrium.

obtained in region (*1*) of 16Y sample, an intense wide luminescence band is observed in the visible region (*1*) of the spectrum with a maximum emission of 2.4 eV (Fig. 5). According to the literature data [14,15], this band is the sum of two bands with emission maximums of 2.2 eV (YB) and 2.7 eV (BB). Based on experimental data on the luminescence of these materials, electrophysical studies, photoelectron spectroscopy and quantum chemical modeling, it was found that single oxygen vacancies [14,16] are causing formation of the band with a maximum luminescence of 2.7 eV in HfO_2, ZrO_2, HfZrO. In paper [15] it was suggested that the band with the emission maximum of 2.2 eV is associated with the formation of oxygen poly-vacancies, presumably di-vacancies.

$^5D_0-^7F_1$ transition is magnetic dipole (MD) transition, and its intensity weakly depends on the local ion environment Eu^{3+}, in contrast to the electrodipole (ED) $^5D_0-^7F_2$ transition. In crystal structures with an inversion center, the intensity of ED $^5D_0-^7F_2$ transition decreases due to the parity prohibition, and the MD transition in the $^5D_0-^7F_1$ luminescence spectrum becomes the most intense [12]. The relationship $I_{((ED)}/I_{(MD)}$ is called an asymmetry coefficient, and the bigger it, the lower the symmetry of the local position occupied by Eu^{3+}. According to the method proposed in the paper [12], the asymmetry coefficient was calculated for all samples (Table 2). We see that asymmetry coefficient max $I_{(ED)}/I_{(MD)}$ (ratio of maxima of intensities

Table 2. Asymmetry coefficients and decay times of transition $^5D_0-^7F_1$

Parameters of the function	16Y(1)	16Y(2)	20Y	24Y	26Y
max $I_{(ED)}/I_{(MD)}$	0.95	0.96	0.98	1.01	1.04
A_1	0.48 ± 0.04	0.47 ± 0.06	0.48 ± 0.06	0.50 ± 0.03	0.49 ± 0.03
t_1,],ms	0.19 ± 0.03	0.07 ± 0.02	0.28 ± 0.06	0.28 ± 0.04	0.27 ± 0.03
A_2	0.52 ± 0.05	0.53 ± 0.01	0.52 ± 0.06	0.50 ± 0.06	0.51 ± 0.03
t_2, ms	1.18 ± 0.06	1.02 ± 0.07	1.36 ± 0.06	1.34 ± 0.07	1.28 ± 0.04

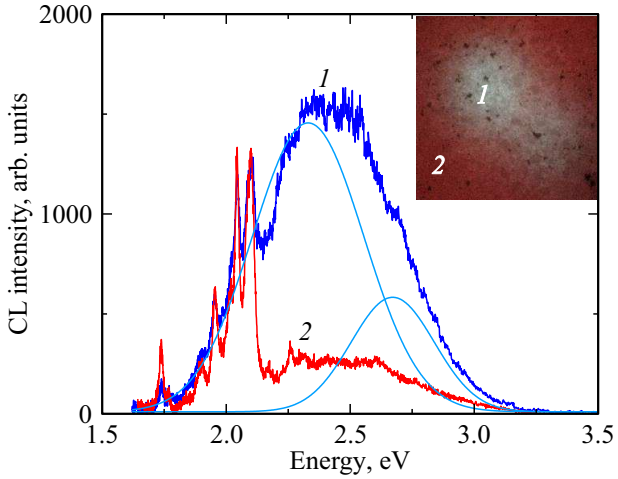

Figure 5. CL image (shown in the insert window) and spectra of sample 16Y obtained in different areas: *1* — white luminescence domain, *2* — red luminescence domain.

of $^5D_0-^7F_2$ and $^5D_0-^7F_1$ bands) is very sensitive to yttrium content.

When zirconium oxide is stabilized by rare-earth elements, the Zr^{4+} ion is replaced in a heterovalent way by a trivalent rare-earth ion with the formation of an oxygen vacancy V_o. At the same time, the different location of vacancies relative to rare earth elements in the near coordination spheres determines the diversity of its environment and the change in its local symmetry. According to the studies [17,18], in zirconium oxide stabilized with yttrium in the cubic phase and activated with Eu^{3+}, the Eu^{3+} ion can be found in several non-equivalent positions. The most symmetrical position with $D2d$ symmetry is formed by an environment of 8 oxygen atoms (CN8). As the concentration of the oxide stabilizer increases, the concentration of oxygen vacancies increases, which leads to the formation of various types of Eu^{3+} local environment. When a vacancy appears in the second coordination sphere, the local symmetry of the center decreases to C_1. When a vacancy occurs in the Eu^{3+} first coordination sphere the local position corresponds to C_{2v} or less. At high concentrations of the stabilizing oxide, 2 vacancies at a time can be observed in the Eu^{3+} first coordination sphere, in this case its local position will correspond to C_2 [17,18].

In [17], it was shown that as the yttrium content increases, the number of centers with lower symmetry goes up, and the intensity of the electrodipole $^5D_0-^7F_2$ transition band rises accordingly. Since hafnium is a chemical analog of zirconium and its ionic radius does not differ significantly, a similar behavior should be Eu^{3+} expected. Thus, the rise of the asymmetry coefficient with an increase in the yttrium content can be explained by higher number of less Eu^{3+} symmetrical positions.

The decay times were obtained for the most intense transition $^5D_0-^7F_1$ (Table 2). It is shown that kinetic curves are well approximated by the sum of two exponentials, which is typical for ceramics:

$$I = I_0 + A_1 \exp\left(-\frac{t}{\tau_1}\right) + A_2 \exp\left(-\frac{t}{\tau_2}\right). \qquad (1)$$

We associate the short component of the decay kinetics with the centers located close to the grain boundaries [12,19]. The transition times of $^5D_0-^7F_1$ in 16Y sample with the lowest yttrium content are noticeably shorter than in the other samples, which indicates a higher content of point defects in this sample. It can be seen that the decay times and their contributions do not depend on the yttrium content at concentrations above 0.2 form units.

Conclusions

The ceramics HfO_2-Y_2O_3-Eu_2O_3 with yttrium content from 0.16 to 0.26 form. units was synthesized. Measurements using EPMA and X-ray diffraction methods showed that a solid solution with a homogeneous composition is formed in the selected concentration range. It is shown that, under the selected synthesis conditions, an increase in the yttrium content leads to the disappearance of minor phases with the yttrium content of more than 0.2 form. units.

In a sample with yttrium content of 0.16 form. units, the domains with an increased content of oxygen vacancies were formed. An increase in the yttrium content leads to a higher number of Eu^{3+} low-symmetry positions.

Funding

E.V. Dementeva, G.A. Gusev and P.A. Dementev would like to thank the Russian Science Foundation for the support (Project № 23-23-00465).

Conflict of interest

The authors declare no conflict of interest.

References

[1] X. Hong, S. Xu, X. Wang, D. Wang, S. Li, B.A. Goodman, W. Deng. J. Lumin., **231**, 117766 (2021). DOI: 10.1016/j.jlumin.2020.117766
[2] X. Wang, X. Tan, S. Xu, F. Liu, B.A. Goodman, W. Deng. J. Lumin., **219**, 116896 (2020). DOI: 10.1016/j.jlumin.2019.116896
[3] S. Stepanov, O. Khasanov, E. Dvilis, V. Paygin, D. Valiev, M. Ferrari. Ceram. Int., **47**, 6608 (2021). DOI: 10.1016/j.ceramint.2020.10.250
[4] M. Eibl, S. Shaw, D. Prieur, A. Rossberg, M.C. Wilding, C. Hennig, K. Morris, J. Rothe, T. Stumpf, N. Huittinen. J. Mater. Sci., **55**, 10095 (2020). DOI: 10.1007/s10853-020-04768-3
[5] L.J. Espinoza-P?rez, E. L?pez-Honorato, L.A. González. Ceram. Int., **46** (10, Part A), 15621 (2020). DOI: 10.1016/j.ceramint.2020.03.109
[6] K.-J. Hwang, M. Shin, M.-H. Lee, H. Lee, M.Y. Oh, T.H. Shin. Ceram. Int., **45** (7, Part B), 9462 (2019). DOI: 10.1016/j.ceramint.2018.09.026
[7] A. Loganathan, A.S. Gandhi. J. Mater. Sci., **52**, 7199 (2017). DOI: 10.1007/s10853-017-0956-2
[8] L. Yang, D. Peng, X. Shan, F. Guo, Y. Liu, X. Zhao, P. Xiao. Sens. Actuators B Chem., **254**, 578 (2018). DOI: 10.1016/j.snb.2017.07.092
[9] H.S. Lokesha, M.L. Chithambo. Radiat. Phys. Chem., **172**, 108767 (2020). DOI: 10.1016/j.radphyschem.2020.108767
[10] V.A. Kravets, K.N. Orekhova, M.A. Yagovkina, E.V. Ivanova, M.V. Zamoryanskaya. Opt. Spectrosc., **125** (2018) 188. DOI: 10.1134/S0030400X18080167.
[11] A.A. Shakirova, E.V. Dementeva, T.B. Popova, M.V. Zamoryanskaya. Opt. Spectrosc., **131** (3), 172 (2023). DOI: 10.61011/EOS.2023.05.56509.76-22.
[12] E.V. Dementeva, A.A. Shakirova, K.N. Orekhova, T.B. Popova, M.A. Yagovkina, A.I. Lihachev, P.A. Dementev, I.D. Venevtsev, A.F. Zatsepin, D.S. Koshelev, V.V. Utochnikova, B. E. Burakov, M.V. Zamoryanskaya. J. Alloys Compd., **1007**, 176452 (2024). DOI: 10.1016/j.jallcom.2024.176452
[13] E.V. Ivanova, V.A. Kravets, K.N. Orekhova, G.A. Gusev, T.B. Popova, M.A. Yagovkina, O.G. Bogdanova, B.E. Burakov, M.V. Zamoryanskaya. J. Alloys Compd., **808**, 151778 (2019). DOI: 10.1016/j.jallcom.2019.151778
[14] D.R. Islamov, V.A. Gritsenko, V.N. Kruchinin et al. Phys. Solid State, **60**, 2050 (2018). DOI: 10.1134/S1063783418100098.
[15] E.V. Dementeva, M.V. Zamoryanskaya, V.A. Gritsenko. Opt. Spectrosc., **130** (12), 1563 (2022). DOI: 10.61011/EOS.2025.01.60562.7408-24.
[16] M.H. Park, C.-C. Chung, T. Schenk, C. Richter, M. Hoffmann, S. Wirth, J.L. Jones, T. Mikolajick, U. Schroeder. Adv. Electron. Mater., **4**, 1700489 (2018). DOI: 10.1002/aelm.201800091
[17] M.A. Borik, T.V. Volkova, E.E. Lomonova, V.A. Myzina, P.A. Ryabochkina, N. Yu. Tabachkova, A.N. Chabushkin, Opt. Spectrosc., **122**, 580 (2017). DOI: 10.1134/S0030400X17040087.
[18] J. Dexpert-Ghys, M. Faucher, P. Caro, J. Solid State Chem., **54**, 179 (1984). DOI: 10.1016/0022-4596(84)90145-2
[19] E.V. Dementieva, A.A. Shakirova, P.A. Dementiev, K.N. Orekhova, M.V. Zamoryanskaya. Opt. Spectrosc., **131** (10) 1359 (2023) (in Russian). DOI: 10.61011/EOS.2025.01.60562.7408-24

Translated by T.Zorina